Computer Simulation of Water in Asymmetric Slit-like Nanopores

Alexander Pertsin and Michael Grunze*

Angewandte Physikalische Chemie, Universität Heidelberg, Im Neuenheimer Feld 253, D-69120 Heidelberg, Germany

Received: April 7, 2004; In Final Form: June 27, 2004

The grand canonical Monte Carlo technique was employed to simulate the behavior of water confined in open asymmetric slit-like nanopores, as formed by parallel hydrophilic and hydrophobic walls. Both structureless nonorienting and structured orienting walls were studied. At a chemical potential slightly above its liquid−vapor bulk coexistence value, an unusual phase state of water was observed, characterized by giant fluctuations of the number of water molecules and a wandering liquid−vapor interface.

1. Introduction

The behavior of water in confined geometries has been of considerable interest in recent years. This is explained, on one hand, by the practical importance of confined water systems in biology, geophysics, chemical engineering, and other areas.[1] On the other hand, the interest in confined water has to do with general fundamental problems related to the effect of confinement on the properties and phase behavior of fluids.[1−4] The effects of reduced dimensionality, as well as the competition of fluid−wall and fluid−fluid interactions, lead to shifts in phase coexistence curves and to the appearance of new kinds of phase transitions not found in the bulk phase.

Because of significant difficulties involved in experimental and theoretical studies of confined water, the information about its properties comes largely from computer simulations. Most of the relevant publications were concerned with the behavior of water in pores of slit-like geometry, such that the confined system was infinite in the *x* and *y* dimensions, while being of finite size in the *z* dimension. The models used in describing the water−wall interactions ranged from simple orientation-independent and laterally averaged potentials[2,5] to structured atomistic models of self-assembled monolayers (SAMs)[6,7] and phospholipid bilayers.[8−10] Early simulation work[11] was focused on surface-induced structural changes in adjacent water, such as layering and orientational ordering. Subsequent studies[5,7,12−14] included evaluation of hydration forces, interfacial tension, shear stress, and other quantities as a function of the pore width and the parameters of the water−wall interaction potential.

Extensive simulations of the phase coexistence in confined water were recently reported by Brovchenko et al.[2] for the TIP4P model[15] of water and smooth-walled nanopores of cylindrical and slit-shaped geometry. The water−wall interaction was described by a (9−3) inverse power potential dependent only on the distance of the water oxygen from the pore wall. The water affinity of the walls was controlled by the potential well depth, ϵ, which was varied from 0.39 to 7.7 kcal/mol (to be compared with the binding energy of 6.2 kcal/mol for two TIP4P water molecules). The simulations were carried out by the Gibbs ensemble Monte Carlo technique, in which the coexisting phases were simulated in separate boxes and no explicit interface was present. As expected, the phase behavior of confined water was governed by the water affinity of the walls. Hydrophobic and moderately hydrophilic walls showed a single liquid−vapor coexistence. However, when the strength of the water−wall interaction was increased and became comparable with that of the water−water interaction, layering and prewetting transitions were also observed.

In all of the simulation studies cited above, the slit-like pore was assumed to be symmetric, i.e., the two walls forming the pore were identical. By contrast, the present paper is concerned with asymmetric pores, with one wall being hydrophilic and the other hydrophobic. Such an asymmetric confinement, which is sometimes referred to as a Janus interface, attracts attention in connection with the experimental study by Zhang et al.[16] The authors[16] measured the shear response of a thin water film confined in a surface forces apparatus (SFA) between the surfaces of muscovite mica (hydrophilic) and a methyl-terminated SAM (hydrophobic). The observed shear response proved to be extraordinarily noisy, and in addition, the frequency dependence of the shear modulus indicated the presence of a wide distribution of relaxation processes. Zhang et al.[16] rationalized their observations in terms of competing tendencies of the water film to wet the hydrophilic surface and to dry the hydrophobic one. A result of this competition is a wandering liquid−vapor interface, which reflects the smallness of the free energy cost of a shift in the interface position. The occurrence of such a "soft-mode" phase in a fluid confined between competing walls was theoretically predicted by Parry and Evans[17,18] and then confirmed in a Monte Carlo simulation by Binder et al.[19] for the simple model case of Ising-type systems. It was shown, in particular, that the wanderings of the liquid−vapor interface should be most pronounced when one confining wall would be completely wet by liquid and the other completely wet by vapor (i.e., completely dry) at bulk coexistence. In the case of partial drying, as in the experiments by Zhang et al.[16] ($\theta = 120°$), the liquid−gas interface can be expected to shift to the hydrophobic wall and the fluctuations in its position can be expected to be moderate.

Recently, McCormick[20] reported a canonical ensemble Monte Carlo simulation of a simple lattice gas model of water at a Janus interface. The interaction of a lattice cell with the hydrophobic wall was set to be 0.1 of the cell−cell interaction, which corresponded to a contact angle $\theta = 143°$. The simula-

* Corresponding author: phone 49-6221-54-8461; fax 49-6221-54-6199; e-mail Michael.Grunze@urz.uni-heidelberg.de.

10.1021/jp048467+ CCC: $27.50
Published on Web 09/25/2004

tion[20] showed large fluctuations in the lattice gas density in contact with the hydrophobic wall, and the power spectrum of the fluctuations proved to be similar to that of the experimental shear response.[16] This similarity allowed the author[20] to conclude that the effects observed by Zhang et al.[16] may well be caused by the contact density fluctuations. Note that in the lattice gas simulation[20] no explicit liquid−gas interface was actually present: The interface was defined in a purely formal way, by averaging the distances of the liquid cell closest to and the vapor cell farthest from the hydrophobic wall.

The objective of our computer simulations is to explore the phase behavior of water in asymmetric confinements in order to check the reasonableness of the conjecture of Zhang et al.[16] concerning the wandering liquid−vapor interface. To be close to the conditions of the SFA experiment,[16] we consider an open confined system that is in chemical equilibrium with bulk water at room temperature. The simulations are carried out by the grand canonical Monte Carlo (GCMC) technique, which is most suitable for simulating open confined systems. The known weakness of the GCMC technique is its inability to simulate coexisting liquid and vapor phases simultaneously because any liquid−vapor interface would not correspond to an absolute minimum in the grand potential.[21] Fortunately, as will be seen in the following, this weakness is surmounted in asymmetric confinements, where the coexisting liquid and vapor phases are individually stabilized by the hydrophilic and hydrophobic walls, respectively. Unlike the lattice-gas simulation by McCormick,[20] we use a more realistic, continuous model for water, with the water−water interactions described by the orientation-dependent TIP4P potential.[15]

2. Methods

Interaction Potentials. In calculations of the total potential energy of the system, the summation of the water−water TIP4P potentials was made by use of the spherical cutoff scheme. The applicability of this scheme to simulation of water in slit-like pores was demonstrated earlier by Shelley and Patey.[22] As in our previous simulations,[5−7,14] the Lennard-Jones potentials were cut off at 7.2 Å, whereas the electrostatic interactions were smoothly damped in the range between 7 and 7.5 Å by use of a switching function suggested by Lee and Rossky.[23]

For the water−wall interactions, both smooth and structured models were tried. In the former case, use was made of energy-shifted (9−3) potentials of the form

$$\varphi(z) = \begin{cases} \varphi_{9-3}(z) - \varphi_{9-3}(z_c) & \text{for } z \le z_c \\ 0 & \text{for } z > z_c \end{cases} \qquad (1)$$

where z is the separation of the water oxygen atom from the wall, z_c is the cutoff distance, assumed to be the same as for the water−water Lennard-Jones potential (7.2 Å), and

$$\varphi_{9-3}(z) = \frac{\epsilon}{2}\left[\left(\frac{\zeta}{z}\right)^9 - 3\left(\frac{\zeta}{z}\right)^3\right] \qquad (2)$$

In the latter equation, ϵ and ζ are, respectively, the depth and position of the potential well, such that $\varphi_{9-3}(\zeta) = -\epsilon$. For the interaction of water with the hydrophilic wall, we accepted $\epsilon = 6.2$ kcal mol^{-1} and $\zeta = 3$ Å, i.e., the water−wall interaction strength and equilibrium separation were assumed to be nearly the same as for the water−water interaction. These potential parameters were kept fixed throughout the simulations. For the hydrophobic wall, several distinct potentials were tried, with $\zeta = 3$ Å and ϵ varied from 0.02 to 0.46 kcal mol^{-1}. A purely repulsive potential was also used, as described by the repulsive term of $\varphi(z)$ with $\zeta = 3$ Å and $\epsilon = 0.46$ kcal mol^{-1} (Figure 1). Note that the value of 0.46 kcal mol^{-1} is a typical potential well depth used in computer simulations in describing the interaction of a water molecule with a hydrophobic paraffin surface.[11]

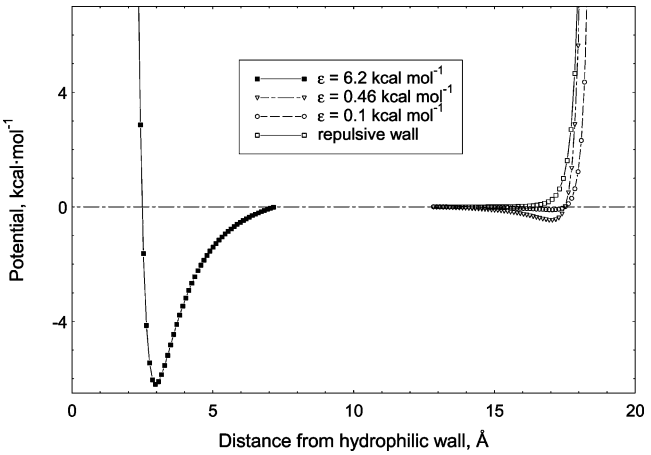

Figure 1. Wall−water potentials used in describing hydrophilic (on the left) and hydrophobic (on the right) structureless walls. (For the hydrophobic wall, only three selected potentials are shown.)

TABLE 1: Potential Parameters for Interaction of Water Molecules with Proton Acceptor Sites on Structured Hydrophilic Wall

interaction	m	n	ϵ (kcal mol^{-1})	ρ (Å)
W···O	8	12	0.44	3.1
W···H	10	12	7.66	1.64

In modeling structured walls, we were not seeking to reproduce the properties of some specific solid surfaces, and so our choice involved a good deal of arbitrariness. As a simple and computationally inexpensive model, we used a hexagonal two-dimensional lattice of force sites hereafter referred to as "wall atoms" or atoms of type W. The lattice period was taken to be 3 Å. The wall atoms were assumed to interact with the individual atoms of water molecules through energy-shifted inverse-power ($n - m$) potentials of the general form

$$\psi(r) = \begin{cases} \psi_{n-m}(r) - \psi_{n-m}(r_c) & r \le r_c \\ 0 & r > r_c \end{cases} \qquad (3)$$

with

$$\psi_{n-m}(r) = \frac{\epsilon}{n-m}\left[m\left(\frac{\rho}{r}\right)^n - n\left(\frac{\rho}{r}\right)^m\right] \qquad (4)$$

In these equations r is the distance between a given wall atom and a particular water atom, r_c is the cutoff radius (7.2 Å), and ϵ and ρ are the well depth and position for the given type of interaction (W···O or W···H).

For the hydrophilic wall, the W···O and W···H potentials were parametrized so as to mimic the ability of the wall atom to behave as a proton acceptor in the hydrogen bond W···H−O with water. The potential parameters used are listed in Table 1, while Figure 2 shows the interaction energy of a water molecule with a wall atom as a function of the W···O separation for some selected orientations of the water molecule. It can be seen that the model potential well reproduces the trend of the W···H−O bond to linear geometry. The potential parameters are scaled so that this bond is energetically equivalent to the linear O··· H−O bond between two TIP4P molecules. In describing the interaction of water with the hydrophobic structured wall, the

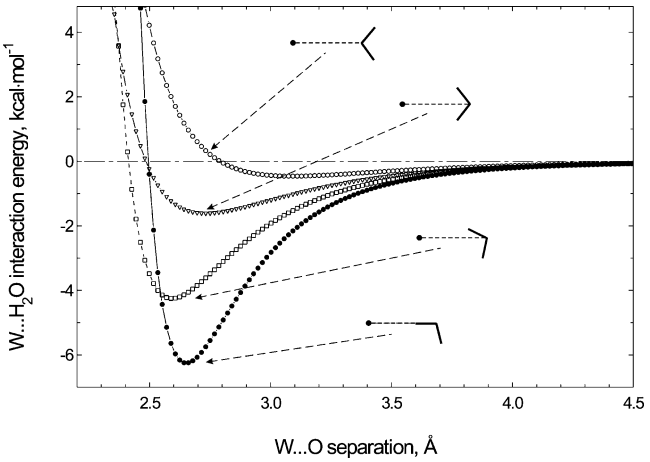

Figure 2. Interaction energy of a water molecule with a proton acceptor site on the structured hydrophilic wall, as a function of O···W separation for some selected water orientations.

W···H interactions were dropped, while the W···O interactions were described by the Lennard-Jones (12−6) potentials with $\rho = 3$ Å and ϵ varied between 0.01 and 0.2 kcal mol^{-1}. A purely repulsive potential decaying with distance as r^{-12} was also tried.

Simulation Procedure. The GCMC procedure used in our simulations is in essence equivalent to that suggested by Adams.[24] The chemical potential of the confined system was specified by setting the "density-corrected" excess chemical potential μ'', as defined by

$$\mu'' = \mu' + kT \ln d \tag{5}$$

In this equation μ' is the excess (configurational) chemical potential[24] and d is the average water density in grams per cubic centimeter, $d = \kappa\langle N\rangle/V$, where $\langle N\rangle$ is the ensemble-averaged number of water molecules and V is the volume of the confined system; if V is expressed in cubic angstroms, then $\kappa = 29.9$ g cm^{-3} Å^3. For bulk water at ambient conditions, d is close to unity and μ'' is practically equal to μ'.

To improve the efficiency of insertions of water molecules, the excluded volume mapping method,[25] closely related to Mezei's cavity-bias technique,[26] is employed. Following this method, the whole volume accessible to the system is divided into a large number of small cubes. A cube is considered to be forbidden for insertion of a new water molecule if there is a water oxygen atom closer than 2.3 Å to all points within the cube. As the simulation proceeds, the state of the cubes is checked and updated. An insertion attempt is accepted with a probability p_{ins}, which can conveniently be written in the form

$$p_{\text{ins}} = \min\left(1, \frac{f_{\text{N}} V \exp[(\mu'' - \Psi_{N+1})/kT]}{(N+1)\kappa b_{\text{ins/del}}}\right) \tag{6}$$

where Ψ_{N+1} is the interaction energy of the inserted molecule with its surrounding molecules and walls, f_{N} is the fraction of cubes allowed for insertion, and $b_{\text{ins/del}}$ is the factor that corrects for the bias when insertions and deletions are attempted with different frequencies.[27] Throughout the simulations, the insertions were attempted 10 times more frequently than deletions, so that $b_{\text{ins/del}} = 10$. The probability of accepting a deletion attempt was calculated from

$$p_{\text{del}} = \min\left(1, \frac{N\kappa b_{\text{ins/del}} \exp[(-\mu'' + \Psi_k)/kT]}{f_{N-1} V}\right) \tag{7}$$

where the subscript k refers to the molecule to be deleted.

Further improvement in sampling efficiency was achieved by use of a Swendsen−Wang filtering technique.[28] The filtering out of energetically unfavorable insertions and deletions was based on a computationally inexpensive predictor of Ψ, in which the electrostatic contribution to the water−water interactions was omitted. When an attempt to insert or delete a water molecule was undertaken, the value of this predictor, hereafter denoted as Ψ^0, was first calculated. Such a tentative attempt was accepted with a probability

$$p^0 = \min(1, \exp\{-\exp[(\Psi^0 - c_1)/c_2 - 1]\}) \tag{8}$$

where the empirical parameters c_1 and c_2 were taken as 12 and 3 kcal mol^{-1}, respectively, following the prescriptions of Shelley and Patey.[27] For a successful Ψ^0-based attempt, the exact interaction energy Ψ was then calculated. The attempt was finally accepted with probabilities p_{ins} or p_{del} corrected for the bias due to filtering.[29]

The simulation box was taken to be a rectangular prism with lateral dimensions L_x and L_y and height h. The hydrophilic and hydrophobic walls were placed at $z = 0$ and $z = h$, respectively, parallel to the $x-y$ plane. In the x and y dimensions, the system was replicated periodically. In the case of structureless walls, we assumed $L_x = L_y = 30$ Å. For structured walls, the simulation box comprised 10 and six rectangular unit cells along the x and y axes, respectively, so that $L_x = 10 \times 3 = 30$ Å and $L_y = 6 \times 2\sqrt{3} \approx 31.2$ Å. The wall-to-wall separation h was varied from 14 Å (i.e., about twice the wall−water potential cutoff) to 40 Å. The length of the GCMC runs ranged from 2×10^6 to 7×10^6 GCMC passes, each comprising N_0 moves, where N_0 is the initial number of molecules in a given pass. For the largest systems studied, the total number of attempted configurations amounted to 5×10^{10}.

In addition to standard distribution functions and ensemble averages calculated in GCMC simulations, we evaluated the z-averaged diagonal components of the Irving−Kirkwood pressure tensor $P_{\alpha\alpha}$ ($\alpha = x, y, z$). The explicit expressions for $P_{\alpha\alpha}$ in terms of the water−water and water−wall interaction potentials can be found elsewhere.[14] The knowledge of the tangential pressure, $P_{\text{T}} = (P_{xx} + P_{yy})/2$, along with the bulk pressure, P_{b}, allowed evaluation of the tension of the confined water film, $\gamma = (P_{\text{b}} - P_{\text{T}})h$. The latter quantity, which is related to the excess grand potential as $\Omega^{\text{ex}} = \gamma L_x L_y$,[3] was used as a criterion in deciding between alternative phase states of confined water.

3. Results and Discussion

Before proceeding to simulations of confined water systems, we examined how well the TIP4P water model, when coupled with the GCMC technique and the accepted cutoff scheme for the interaction potential, reproduced the properties of bulk water at ambient conditions. For the excess chemical potential of TIP4P water, the available literature data range from −5.9 to −6.2 kcal mol^{-1} depending on the simulation method used.[2] To cover this range, we tested some selected values of μ'' between −5.9 and −6.3 kcal mol^{-1}. The best agreement with the experimental bulk water density (0.997 g cm^{-3}) was observed at $\mu'' = -6.103$ kcal mol^{-1}. The respective simulation results were $d = 0.995 \pm 0.002$ g cm^{-3} and $P_{\text{b}} = 0.25 \pm 0.03$ kbar. To fit P_{b} to the atmospheric pressure, μ'' had to be reduced to −6.203 kcal mol^{-1} to result in $P_{\text{b}} = 0.02 \pm 0.03$ kbar and $d = 0.981 \pm 0.002$ g cm^{-3}. Note that the saturated vapor pressure of TIP4P water at room temperature is practically zero (5×10^{-5} kbar),[30] so that the value of $\mu'' = -6.203$ kcal mol^{-1} is

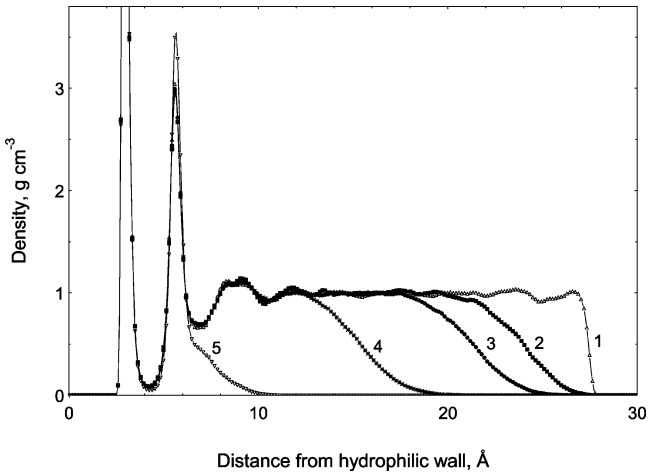

Figure 3. Water density profiles for smooth-walled pores at $\mu'' = -6.105$ kcal mol^{-1} and $h = 30$ Å. Curve 1 corresponds to state 2 + L ($\epsilon = 0.46$ kcal mol^{-1}); curves 2−4, to state 2 + L + V (repulsive wall); and curve 5, to metastable state 2 + V (repulsive wall). The first density maximum is cropped to have better resolution in the hydrophobic part of the profile.

the best what we have for an estimate of the liquid−gas coexistence value of μ'' at room temperature, hereafter μ''_{sat}. It should be realized, however, that P_b is fairly sensitive to simulation details such as the potential cutoff distance, the mode of cutoff (sharp or smooth, energy-shifted or not), and the system size, which are usually different in different simulation studies.[2,30−32] Our test simulations of bulk TIP4P water as a function of these parameters showed that the total uncertainty in P_b (including the statistical uncertainty of 0.03 kbar) may amount to 0.1 kbar. Considering the observed dependence of P_b on μ'', the respective uncertainty in μ''_{sat} can be estimated to be 0.05 kcal mol^{-1}, so that for the most likely range of μ''_{sat} we can accept $\mu''_{sat} = -6.2 \pm 0.05$ kcal mol^{-1}.

We began our simulations of the confined water systems with smooth-walled pores and first tried the least hydrophobic ($\epsilon = 0.46$ kcal mol^{-1}) and the most hydrophobic (purely repulsive) walls. Initially, μ'' was set at -6.105 kcal mol^{-1}, that is, ∼0.05 kcal mol^{-1} above the upper estimated limit for μ''_{sat}. At $\epsilon = 0.46$ kcal mol^{-1}, the system showed nothing unusual in its phase behavior. In the whole range of the pore widths tried, the water density distribution represented a simple combination of two density profiles. As seen from Figure 3, where curve 1 presents the respective water density distribution at $h = 30$ Å, the left part of the density profile is characteristic of liquid water in contact with a hydrophilic wall, whereas the right part is typical of contact with a hydrophobic wall.[5] In Table 2, which summarizes the phase behavior of the system at $\mu'' = -6.105$ kcal mol^{-1}, the state of the system at $\epsilon = 0.46$ kcal mol^{-1} is denoted as 2 + L, where 2 is included in notation to emphasize the presence of two distinct hydration layers at the hydrophilic wall. It is important that the observed density distributions proved to be independent of whether an almost empty pore or a pore filled with liquid water was used to initiate the GCMC run. This suggests that the 2 + L state represents a stable state of the system.

Quite a different phase behavior was observed when the hydrophobic wall was made purely repulsive. At $h = 14$ and 20 Å, water formed two well-defined liquid layers at the hydrophilic wall, while the rest of the pore was occupied with water vapor. The relevant state is denoted in Table 2 as 2 + V. Here again, the final state of the confined system was independent of the starting configuration of the GCMC run:

TABLE 2: Phase States of Water Confined between Competing Walls at $\mu'' = -6.105$ kcal mol^{-1} as a Function of ϵ and h

		final phase state[a]	
ϵ[b] (kcal mol^{-1})	h (Å)	started from L	started from V
	Structureless Walls		
repulsive wall	14, 20	2 + V	2 + V
	30, 40	2 + L + V	(2 + V)
$0.1 < \epsilon \le 0.46$	14, 30, 40	2 + L	2 + L
$\epsilon \le 0.1$	30	2 + L + V	(2 + V)
	Structured Walls		
$\epsilon > 0.05$	30	1 + L	(1 + V)
$\epsilon \le 0.05$	14	1 + V	1 + V
	30	1 + L + V	(1 + V)
repulsive wall	14, 20	1 + V	1 + V
	30	1 + L + V	(1 + V)

[a] See the text for designation of the phase states. Metastable states are enclosed in parentheses. [b] For structureless walls, ϵ refers to the interaction of a water molecule with the whole hydrophobic wall, whereas for structured walls it relates to the interaction with a single force site on the hydrophobic wall.

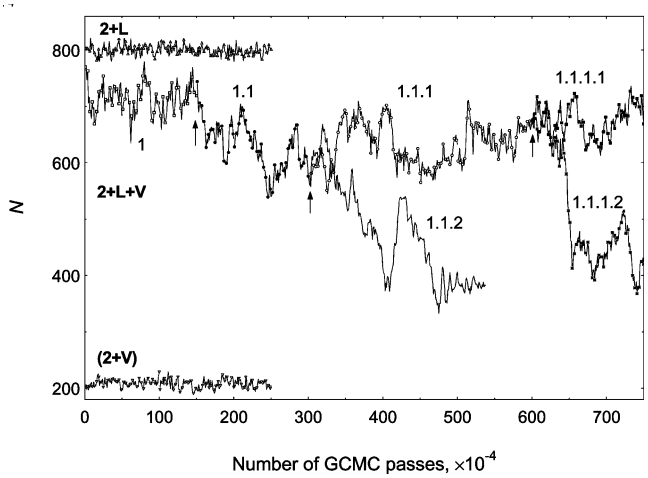

Figure 4. Behavior of the number of water molecules during the GCMC run at $\mu'' = -6.105$ kcal mol^{-1} and $h = 30$ Å for 2 + L state ($\epsilon = 0.46$ kcal mol^{-1}), 2 + L + V state (repulsive wall), and metastable 2 + V state (repulsive wall). The numbers at the curves label different runs (see text for notations), while the arrows show the junctions of successive runs. In this and similar figures in the following, the data points represent the magnitude of N in the end of every 10^4 GCMC passes, while the markers, if available, are set at every third data point just to better distinguish different curves.

Both liquid and vapor configurations led eventually to the 2 + V structure. At larger pore widths (30 and 40 Å), a fairly thick and nearly homogeneous liquid layer arose between the vapor phase adjacent to the hydrophobic wall and the two monolayers adsorbed on the hydrophilic wall. In Table 2, this state is referred to as 2 + L + V, and the relevant density profiles for $h = 30$ Å are shown in Figure 3 (curves 2−4). This 2 + L + V state was only observed when the GCMC run was started from a liquid configuration, whereas any vapor configuration resulted in a 2 + V state (Figure 3, curve 5). The choice between these alternatives was made on the basis of the magnitude of the water film tension γ, which favored the 2 + L + V state by more than 15 dyn cm^{-1} (see below).

A remarkable feature of the 2 + L + V state was the occurrence of unusually large fluctuations in the number of water molecules during the GCMC run. This feature can be appreciated from Figure 4, which illustrates the behavior of N as the GCMC simulation progresses. The different curves presented

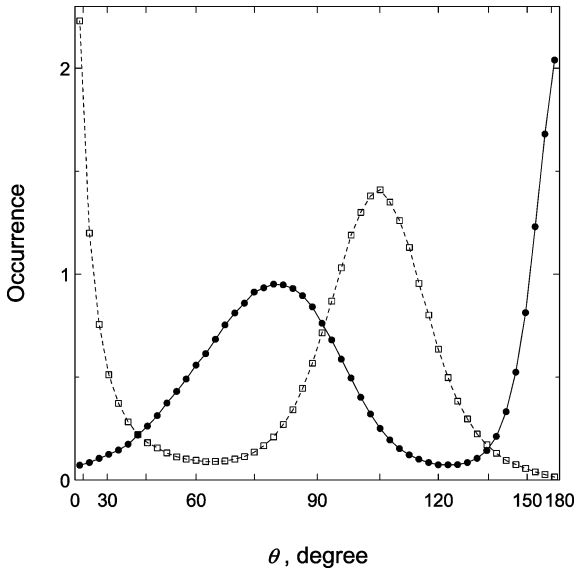

Figure 5. Orientational distribution of OH bonds in the first hydration layer near the hydrophilic wall for smooth nonorienting walls (□) and structured proton-acceptor walls (●).

for state 2 + L + V refer to different GCMC runs. (The notation of the runs is the following: Run 1.1 is a continuation of run 1, runs 1.1.1 and 1.1.2 are two independent continuations of run 1.1 and so forth.) For comparison, a typical behavior of N during the GCMC run for the 2 + L and 2 + V states is also shown. Aside from a much larger scatter of N in the relatively stable sections of the curves, the 2 + L + V state is characterized by occasional instabilities seen as jumps of N onto noticeably different average levels. The giant fluctuations of N observed in the 2 + L + V state manifested themselves in the water density distribution as a wandering L−V interface. This is seen from Figure 3, where curves 2, 3, and 4 present the density profiles for runs 1.1.1.1, 1.1, and 1.1.1.2, respectively. The film tensions γ corresponding to these profiles were calculated to be −125, −136, and −130 ± 5 dyn cm^{-1}, that is, the variations in γ were masked by the statistical uncertainty involved in evaluation of γ.[33] The metastable 2 + V state had $\gamma = -109 \pm 5$ dyn cm^{-1}, well above the range characteristic of the 2 + L + V state.

The introduction of a slight attraction between water and the hydrophobic wall had an effect dependent on the magnitude of ϵ (see Table 2). At $\epsilon > 0.1$ kcal mol^{-1}, the phase behavior of the confined water was the same as discussed above for $\epsilon =$ 0.46 kcal mol^{-1}, with the stable state being 2 + L. As ϵ was reduced to 0.1 kcal mol^{-1} and below, a 2 + L + V phase state, similar to that found for the repulsive hydrophobic wall, was again observed. Note that the well depth of 0.1 kcal mol^{-1} constitutes only 0.016 of the water−water binding energy, so that the hydrophobic wall is most likely in compliance with the complete drying condition.

To make sure that the soft-mode state characterized by large fluctuations of N and a wandering L−V interface is not a specific feature of the smooth structureless walls used in the simulations, we tried structured walls with the orientation-dependent wall−water potentials described in the previous section. The effect of these walls on the structure of adjacent water was substantially different from that of the structureless (9−3) walls. This can be appreciated from Figure 5, which compares the orientational distributions of water OH bonds near the hydrophilic wall for the smooth and structured cases. The abscissa axis shows the angle θ formed by the OH bond and

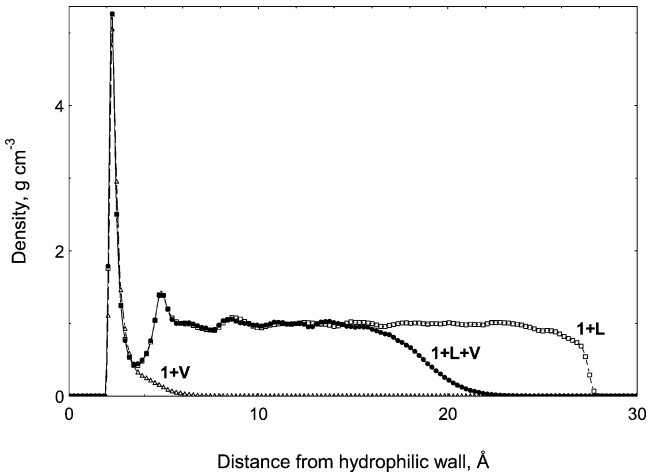

Figure 6. Water density profiles for the 1 + L, 1 + L + V, and 1 + V phase states found at $\mu'' = -6.105$ kcal mol^{-1} and $h = 30$ Å for structured walls (see Table 2 for the associated parameters of the hydrophobic wall).

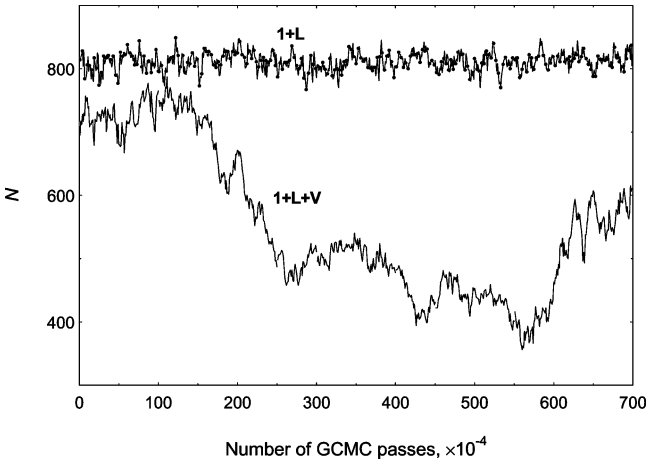

Figure 7. Behavior of the number of water molecules during GCMC run for structured walls at $\mu'' = -6.105$ kcal mol^{-1} and $h = 30$ Å. The 1 + L and 1 + L + V states refer, respectively, to the hydrophobic force sites with $\epsilon = 0.1$ kcal mol^{-1} and the purely repulsive force sites.

the normal to the hydrophilic wall, so that the values $\theta = 0°$ and 180° correspond to directions outward and toward the wall, respectively. At the structureless wall, the preferred direction of the OH bond is outward from the wall. This is typical of nonorienting walls, where the preferred orientation of adjacent water molecules is dictated by their trend to maximize the number of hydrogen bonds with neighboring water molecules.[14] By contrast, the structured wall, which carries a lattice of proton-acceptor sites, forces the adjacent water molecules to orient their OH bonds toward the wall. Another difference between the structured and structureless walls can be seen from Figure 6, which presents the water density profiles for the three phase states found in the case of the structured walls at $\mu'' = -6.105$ kcal mol^{-1} (see Table 2). In all of the states, there is only one hydration layer next to the hydrophilic wall, which is a consequence of the shorter range and strong orientation dependence of the wall−water potential used. Despite this difference, a soft-mode state characterized by giant fluctuations of N was again observed (Figure 7).

To gain a better insight into the nature of the unusual soft-mode state, we carried out a series of simulations as a function of μ''. In these simulations, we restricted ourselves to smooth-walled pores and a single pore width of $h = 30$ Å. Most simulations were concerned with the purely repulsive hydro-

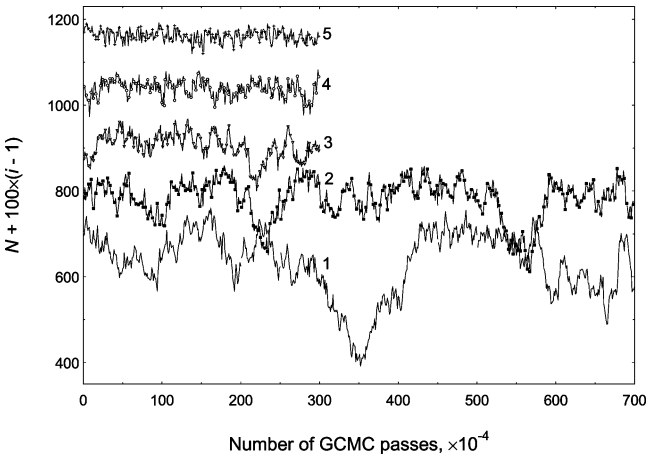

Figure 8. Behavior of the number of water molecules during GCMC run for smooth-walled pores with purely repulsive hydrophobic wall at $h = 30$ Å as a function of μ''. Curves 1−5 are for $\mu'' = -6.0$, -6.05, -6.09, -6.095, and -6.1 kcal mol^{-1}, respectively. To avoid overlap, each curve is shifted up by $100(i - 1)$, where i is the curve number.

TABLE 3: Phase States of Water Confined between Competing Structureless Walls at $h = 30$ Å as a Function of μ''

		final phase state	
μ'' (kcal mol^{-1})	ϵ (kcal mol^{-1})	started from L	started from V
−6.0, −6.05	repulsive wall	2 + L	2 + L
−6.09		2 + L	(2 + V)
−6.095, −6.1, −6.105, −6.11		2 + L + V	(2 + V)
−6.13, −6.15, −6.22		2 + V	2 + V
−6.22	$\epsilon < 0.51$	2 + V	2 + V
	$\epsilon \geq 0.51$	2 + L	(2 + V)

phobic wall. A total of 10 values of μ'' were tried, spanning the range from −6.0 to −6.22 kcal mol^{-1} (Table 3). The effect of μ'' on the variations in N during the GCMC run can be appreciated from Figure 8, which presents the results for $\mu'' \geq$ 6.1 kcal mol^{-1}. To avoid overlap, the next to the lowest curve is shifted up by 100, the following one by 200, and so on. At $\mu'' = -6.0$ kcal mol^{-1}, the magnitude of the fluctuations in N is practically the same as observed for a typical 2 + L state at $\mu'' = -6.105$ kcal mol^{-1} (see, for example, the uppermost curve in Figure 4). As μ'' is reduced, the fluctuations get more and more pronounced until the behavior of N becomes, at $\mu'' = -6.1$ kcal mol^{-1}, similar to that discussed above for the 2 + L + V state at $\mu'' = -6.105$ kcal mol^{-1}. The observed changes in the magnitude of fluctuations can be appreciated quantitatively from Figure 9, which shows the rms deviation of N, σ_N, from its mean value as a function of μ''. It can be seen that σ_N grows by almost an order of magnitude as μ'' approaches −6.105 kcal mol^{-1}. It is noteworthy that in the 2 + L region the growth in the fluctuations of N occurs mostly in a fairly thin layer adjacent to the hydrophobic wall. By use of the terminology of the lattice gas simulation study by McCormick,[20] these growing fluctuations can be referred to as the fluctuations in the contact density of water. The growth in the magnitude of these fluctuations manifests itself in blurring of the hydrophobic edge of the water density profile, as clearly observed in Figure 10.

As μ'' is reduced to −6.11 kcal mol^{-1}, a transition from the 2 + L + V to the 2 + V phase state occurs; that is, the fluctuating liquid water layer evaporates. If our estimate for the upper limit of μ''_{sat} is correct and so the evaporation takes place on the liquid side of the liquid−vapor bulk coexistence, the 2 + L + V to 2 + V transition may be regarded as a partial capillary evaporation (i.e., occurring not in the whole available

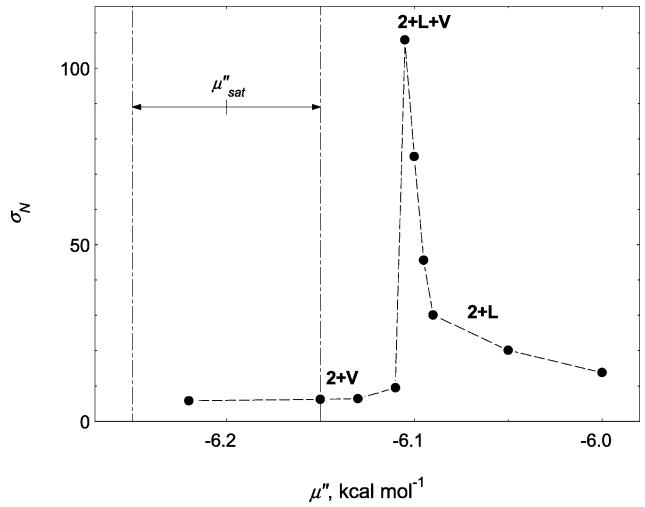

Figure 9. Rms deviation of N from its ensemble average $\langle N \rangle$ during GCMC run as a function of μ'' for smooth-walled pores with purely repulsive hydrophobic wall.

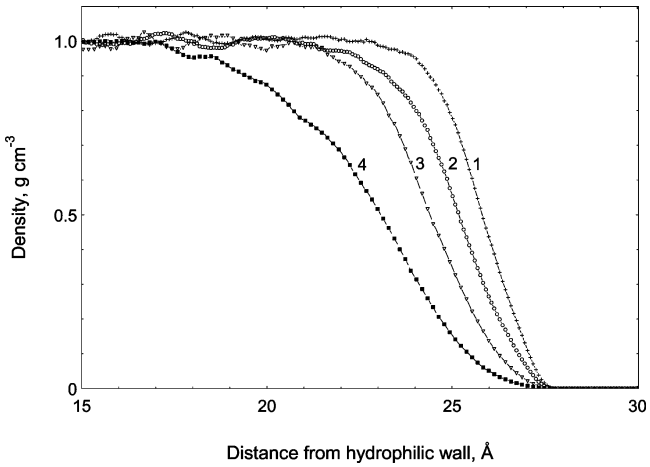

Figure 10. Hydrophobic edges of the water density profiles for smooth-walled pores with purely repulsive hydrophobic wall as a function of μ''. Curves 1−4 are for $\mu'' = -6.0$, -6.05, -6.09, and -6.095 kcal mol^{-1}, respectively.

volume). To check whether the 2 + L + V state can be recovered by increasing the water affinity of the hydrophobic wall, we carried out a series of simulations at $\mu'' = -6.22$ kcal mol^{-1} as a function of ϵ (see Table 3). For moderately attracting hydrophobic walls ($\epsilon < 0.51$ kcal mol^{-1}), the stable state of the system was 2 + V, as for the purely repulsive hydrophobic wall. At $\epsilon \geq 0.51$ kcal mol^{-1}, a capillary condensation occurred, thus attesting that we are on the vapor side of the liquid−vapor coexistence, and so our lower estimate for μ''_{sat} is a little too low. In none of the simulations at $\mu'' = -6.22$ kcal mol^{-1} have we observed the 2 + L + V state with an enormously fluctuating N and a wandering L−V interface.

As with the simulations at a fixed μ'' (Table 2), the final phase state of the system in the μ''-dependent simulations was sensitive to the starting configuration. This can be seen from Table 3, where the metastable states are enclosed in parentheses. The difference in γ between the stable and metastable states ranged from 15 to 35 dyn cm^{-1}.

4. Conclusion

Prompted by the experimental findings of Zhang et al.,[16] we undertook GCMC simulations of water in asymmetric slit-like nanopores, as formed by parallel hydrophilic and hydrophobic

walls. Unlike the case of bulk and symmetrically confined systems, the GCMC technique proved to be capable of explicitly simulating the liquid−vapor interface for water in the asymmetric confinement. The obvious reason is that the coexisting liquid and vapor waters are individually stabilized by the hydrophilic and hydrophobic walls, respectively, which facilitates simulation of the liquid−vapor coexistence.

In a narrow range of μ'' slightly above the upper estimate of μ''_{sat}, an unusual soft-mode state of confined water, as characterized by giant fluctuations of N and a wandering liquid−vapor interface, was found. When relating this state to the experimental observations by Zhang et al.,[16] it should however be kept in mind that in our simulations the wandering interface was observed with completely dried hydrophobic walls, in agreement with the theoretical predictions by Parry and Evans.[17,18] By contrast, the SFA experiments[16] were made with a partially dried wall. In this case the liquid−vapor interface can be expected to be close to the hydrophobic wall and the fluctuation effects should be much less pronounced. Also, it is not unlikely that no liquid−vapor interface was present in the experiments of Zhang et al.[16] at all, and the extraordinarily noisy shear response originated from large fluctuations in the contact water density, similar to those observed in our simulations for the 2 + L phase at $\mu'' \geq -6.095$ kcal mol $^{-1}$ (Figure 10). The ability of such fluctuations to cause the effects observed by Zhang et al.[16] has been demonstrated in the lattice gas simulations by McCormick.[20]

Acknowledgment. We are grateful to R. Evans for critical reading of the manuscript and valuable suggestions. We also thank S. Granick for helpful discussions. This research was supported by the Deutsche Forschungsgemeinschaft and the Office for Naval Research.

References and Notes

(1) Gelb, L. D.; Gubbins, K. E.; Radhakrishnan, R.; Sliwinska-Bartkowiak, M. *Rep. Prog. Phys.* **1999**, *62* (12), 1573−1659.
(2) Brovchenko, I.; Geiger, A.; Oleinikova, A. *J. Chem. Phys.* **2004**, *120* (4), 1958−1972.
(3) Evans, R.; Marconi, U. M. B. *J. Chem. Phys.* **1987**, *86* (12), 7138−7148.
(4) Evans, R. *J. Phys.: Condens. Matter* **1990**, *2* (46), 8989−9007.
(5) Hayashi, T.; Pertsin, A. J.; Grunze, M. *J. Chem. Phys.* **2002**, *117* (13), 6271−6280.
(6) Pertsin, A. J.; Grunze, M. *Langmuir* **2000**, *16* (23), 8829−8841.
(7) Pertsin, A. J.; Hayashi, T.; Grunze, M. *J. Phys. Chem. B* **2002**, *106* (47), 12274−12281.
(8) Tobias, D. J.; Tu, K.; Klein, M. L. *Curr. Opin. Colloid Interface Sci.* **1997**, *2* (1), 15−26.
(9) Saiz, L.; Klein, M. L. *Acc. Chem. Res.* **2002**, *35* (6), 482−489.
(10) Pandit, S. A.; Berkowitz, M. L. *Biophys. J.* **2002**, *82* (4), 1818−1827.
(11) Lee, C. Y.; McCammon, J. A.; Rossky, P. J. *J. Chem. Phys.* **1984**, *80* (9), 4448−4455.
(12) Wallqvist, A.; Berne, B. J. *J. Phys. Chem.* **1995**, *99* (9), 2893−2899.
(13) Koga, K. *J. Chem. Phys.* **2002**, *116* (24), 10882−10889.
(14) Pertsin, A. J.; Grunze, M. *J. Phys. Chem. B* **2004**, *108* (4), 1357−1364.
(15) Jorgensen, W. L.; Chandrasekhar, J.; Madura, J. D.; Impey, R. W.; Klein, M. L. *J. Chem. Phys.* **1983**, *79* (2), 926.
(16) Zhang, X.; Zhu, Y.; Granick, S. *Science* **2002**, *295* (5), 663−666.
(17) Parry, A. O.; Evans, R. *Phys. Rev. Lett.* **1990**, *64* (4), 439−442.
(18) Parry, A. O.; Evans, R. *Physica A* **1992**, *181* (3−4), 250−296.
(19) Binder, K.; Landau, D. P.; Ferrenberg, A. M. *Phys. Rev. E* **1995**, *51* (4), 2823−2838.
(20) McCormick, T. A. *Phys. Rev. E* **2003**, *68* (6), 061601.
(21) Peterson, B. K.; Gubbins, K. E.; Heffelfinger, G. S.; Marconi U. M. B.; Swol, F. *J. Chem. Phys.* **1988**, *88* (10), 6487.
(22) Shelley, J. C.; Patey, G. N. *Mol. Phys.* **1996**, *88* (2), 385−398.
(23) Lee, S. H.; Rossky, P. J. *J. Chem. Phys.* **1994**, *100* (4), 3334.
(24) Adams, D. J. *Mol. Phys.* **1974**, *28* (5), 1241−1252.
(25) Stapleton, M. R.; Panagiotopoulos, A. *J. Chem. Phys.* **1990**, *92* (2), 1285−1293.
(26) Mezei, M. *Mol. Phys.* **1980**, *40* (4), 901−906.
(27) Shelley, J. C.; Patey, G. N. *J. Chem. Phys.* **1995**, *102* (19), 7656−7662.
(28) Swendsen, R. H.; Wang, J.-S. *Phys. Rev. Lett.* **1987**, *58* (2), 86−88.
(29) The correction is accomplished by multiplying $b_{ins/del}$ in eqs 6 and 7 by p^0.
(30) Cracknell, R. F.; Nicholson, D.; Parsonage, N. G.; Evans, H. *Mol. Phys.* **1990**, *5* (4), 931.
(31) Lísal, M.; Smith, W. R., Nezbeda, I. *Fluid Phase Equilib.* **2001**, *181* (1−2), 127−146.
(32) Vorholz, J.; Harismiadis, V. I.; Rumpf, B.; Panagiotopoulos, A. Z.; Maurer, G. *Fluid Phase Equilib.* **2000**, *170* (2), 203−234.
(33) In calculations of γ from the transversal pressure, the statistical uncertainty in γ grows linearly with h as $\delta\gamma = \delta Ph/2$. For $h = 30$ Å and $\delta P = 0.03$ kbar, this results in $\delta\gamma \approx 5$ dyn cm^{-1}.